Received: 1 March 2021 | Accepted: 9 July 2021

DOI: 10.1111/tbed.14234

Transboundary and Emerging Diseases WILEY

ORIGINAL ARTICLE

A computational study of the interface interaction between SARS-CoV-2 RBD and ACE2 from human, cat, dog, and ferret

William O. Soté[1] | Eduardo F. Franca[1] | Aline S. Hora[2] | Moacyr Comar Jr.[1]

[1] Chemistry Institute, Federal University of Uberlandia, Minas Gerais, Brazil

[2] School of Veterinary Medicine, Federal University of Uberlandia, Minas Gerais, Brazil

Correspondence
Moacyr C. Jr., Chemistry Institute, Federal University of Uberlandia, Minas Gerais 38400-902, Brazil.
Email: mcomjr@gmail.com

Abstract

The total impact of the worldwide COVID-19 pandemic is still emerging, changing all relationships as a result, including those with pet animals. In the infection process, the use of angiotensin-converting enzyme 2 (ACE2) as a cellular receptor to the spike protein of the new coronavirus is a fundamental step. In this sense, understanding which residue plays what role in the interaction between SARS-CoV-2 spike glycoprotein and ACE2 from cats, dogs, and ferrets is an important guide for helping to choose which animal model can be used to study the pathology of COVID-19, and if there are differences between these interactions and those occurring in the human system. To help answer these questions, we performed classical molecular dynamics simulations to evaluate, from an atomistic point of view, the interactions in these systems. Our results show that there are significant differences in the interacting residues between the systems from different animal species, and the role of ACE2 key residues are different in each system, and can assist in the search for different inhibitors for each animal.

KEYWORDS
angiotensin-converting enzyme 2, molecular dynamics, receptor binding domain, Severe acute respiratory syndrome coronavirus 2

1 | INTRODUCTION

The emergence of a new coronavirus (Morens et al., 2020; Wu et al., 2020; Zhou et al., 2020; Zhu et al., 2020) with high infection capacity clearly shows that there is an increasing need to study many aspects of this pathogen. A key point during infection is cellular attachment of the virus, mediated by interaction between the SARS-CoV-2 receptor binding domain (RBD), which plays a pivotal role in host selectivity (Li, 2015; Li et al., 2003), and host angiotensin-converting enzyme 2 (ACE2) receptor. The origin of the new coronavirus has been demonstrated to be a species of bat (Cui et al., 2019; Li et al., 2006), but recent reports suggest that animals which share some specific residues in ACE2 could be hosts of SARS-CoV-2, including cats, dogs, and ferrets (Luan et al., 2020). Hence, considering the large population and economic importance of companion animals (Gapper, 2019), and the difference in their ACE2 sequences (Figure 1), it is important to understand what the role of these ACE2 key residues is, in the interaction process between SARS-CoV-2 RBD and ACE2, because the participation of companion animals in the epidemiological chain of COVID-19 transmission remains in debate (Hora, 2020; Mallapaty, 2020; Shi et al., 2020; Sit et al., 2020).

In this sense, an evaluation of this process from an atomistic point of view can provide important information about the role of these specific residues; and the use of in silico strategies to simulate the interaction of proteins is ubiquitous, mainly using molecular docking and molecular dynamics simulations, since the advancement of both hardware and software has allowed for the study of bigger and larger systems (Perilla & Schulten, 2017). In the case of the new coronavirus pandemic, molecular docking and classical molecular simulation have been used in some studies to evaluate different aspects of the virus (Arantes et al., 2020; Basu et al., 2020; Razzaghi-Asl et al., 2020). Considering the specific differences in ACE2, we performed homology modeling, molecular docking, and molecular dynamics simulations to observe the behavior of the interaction interface involving the RBD and ACE2 proteins for

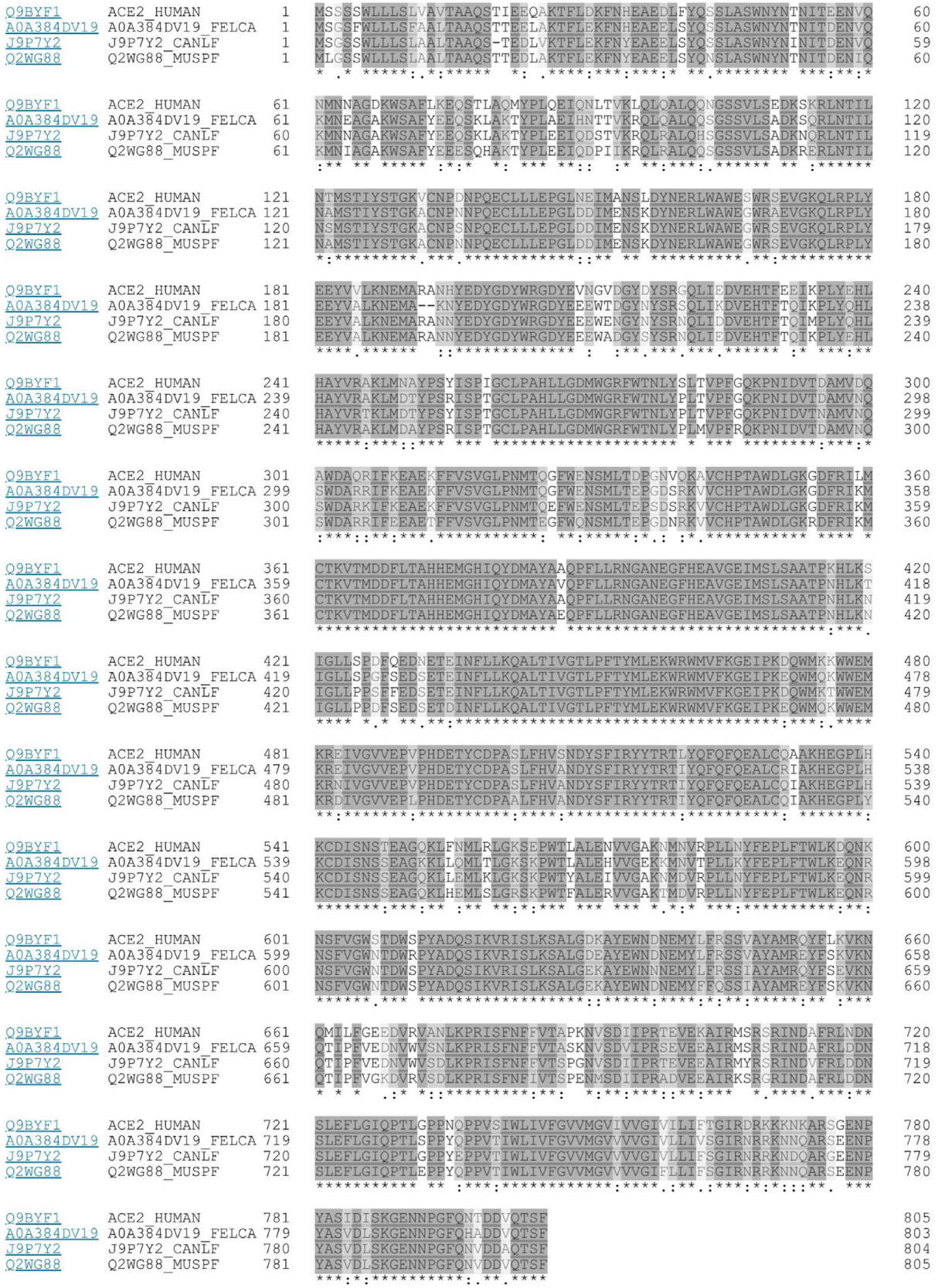

FIGURE 1 Multiple sequence alignment of human (Q9BYF1), cat (A0A384DV19), dog (J9P7Y2), and ferret (Q2WG88) angiotensin-converting enzyme 2 (ACE2) receptor. Differences between sequences are light gray or white, considering sequence of human ACE2 as a reference

TABLE 1 Haddock results for the studied systems. Z-score negative values indicate better docking of the structures

System	HADDOCK score	Z-score
Cat	-58.5 ± 5.0	−2.2
Dog	-34.5 ± 8.5	−2.2
Ferret	-19.8 ± 8.9	−2.2
Human (redocking)	-10.5 ± 6.7	−1.9

human (*h*ACE2), cat (*c*ACE2), dog (*d*ACE2), and ferret (*f*ACE2) systems. This is, as far we know, the first study of its kind.

2 | MATERIALS AND METHODS

2.1 | Homology modeling and docking procedures

The structure used for the human system was SARS-CoV-2 RBD complexed with human receptor ACE2 (PDB: 6LZG). For cat (Uniprot: Q56H28), dog (Uniprot: J9P7Y2), and ferret (Uniprot: Q2WG88) systems, the FASTA sequences of ACE2 receptors were used in the Swiss Model webserver (Waterhouse et al., 2018) to build models which were equilibrated by a 1 ns simulation (details in section 2.2). The quality of all the models was confirmed with the help of Ramachandran plots (Figure S1 in the Supporting Information), using PROCHECK online server (Laskowski et al., 1993). The amino acid sequence of the SARS-CoV-2 spike obtained from human (Uniprot: P0DTC2) was compared with those obtained from dogs (GenBank: QIT08256.1; QIT08292.1) and cats (GenBank; QOF07648.1; QLG96797.1) naturally infected with SARS-CoV-2, to assess possible differences in RBD by visual comparison after alignment using the BioEdit 7.0.5.3 software (Hall, 1999). No SARS-CoV-2 spike sequences from naturally infected ferrets were found in the public database. In RBD, differences between amino acids from human, dog, and cat were not found (Figure S2 in the Supporting Information). Finally, the SARS-CoV-2 RBD and the non-human receptors were docked using HADDOCK 2.4. (Van Zundert et al., 2016). The docking was performed under default settings, where random removal of ambiguous interaction restraints (AIRs) was switched on; the number of trials for rigid body minimization was five; the number of structures for rigid body docking (it0) was 1000, and the semi-flexible residues were automatically defined based on intermolecular contacts that were less than 5 Å. The fraction of common contacts (FCC) clustering parameters used were 0.6 for cut-off and 4 for minimum cluster size. The docking results are given in Table 1.

2.2 | Molecular dynamics simulations

The Protein Data Bank (PDB) format of the docked systems, described in Section 2.1, were placed in a rectangular cuboid simulation box and were solvated by filling the box with Three Site Transferrable Intermolecular Potential (TIP3P) water model (Jorgensen et al., 1983) molecules. Sodium and chloride ions were used to neutralize the total charge of the macromolecules. Molecular dynamics simulations were carried out using GROMACS 2016.4 (Abraham et al., 2015) and OPLS-AA force field (Jorgensen & Tirado-Rives, 1988). All systems were simulated in triplicate to ensure reliability in the simulation and the obtained results (Figure S3–S6 in the Supporting Information confirmed reproducibility). Each system was then energy minimized using 50,000 steps of the steepest descent method, and a convergence criterion with a maximum force of 1000 kJ mol^{-1} nm^{-1}, followed by two steps of solvent equilibration with all non-hydrogen protein atoms constrained by a force constant of 1000 kJ mol^{-1} nm^{-2}. The first equilibration consisted of a molecular dynamics simulation performed by 125 ps in an isochoric–isothermal (NVT, number of particles, volume, and temperature) ensemble at 310 K, maintained using velocity-rescale coupling method (Bussi et al., 2007), with a coupling time constant of 0.1 ps; the second equilibration was performed in an isobaric–isothermal (NPT, number of particles, pressure, and temperature) ensemble at 1.0 bar, isotropically applied and maintained by the Berendsen weak coupling method (Berendsen et al., 1984), with a coupling time constant of 0.5 ps and compressibility of 4.5×10^{-5} bar^{-1}. Each production step of 50 ns used a time step of 1 fs with no position restraints; the temperature was maintained at 310 K using a Nosé–Hoover thermostat (Hoover, 1985; Nosé, 1984) with a coupling time constant of 0.2 ps. Pressure was maintained at 1.0 bar using a Parrinello–Rahman barostat (Nosé & Klein, 1983; Parrinello & Rahman, 1981) with a coupling time constant of 0.5 ps. All bonds' stretching and bending motions were constrained using LINCS algorithm (Hess et al., 1997). Long-range electrostatics were evaluated using particle-mesh Ewald (PME) method, and a 1.0 nm cut-off was considered for short-range interactions. All analyses were performed with GROMACS and VMD software (Humphrey et al., 1996).

3 | RESULTS

Using the described methodology, the following results were obtained to the structural and interaction behavior for the studied systems.

3.1 | Root-mean-square fluctuation and number of hydrogen bond analysis

All simulations were done in triplicate of 50 ns each, totalizing 600 ns of simulation, and the first analysis, shown in Figure 2, is the average root-mean-square fluctuation (RMSF) for ACE2 interacting residues (the results for all replicas are in Figures S3–S6 in the Supporting Information). The RMSF evaluates the flexibility of the residues by computing the variance of the fluctuations around the average position, $\langle r_i \rangle$, and can be obtained by the equation:

$$\rho_i^{\mathrm{RMSF}} = \sqrt{\langle (r_i - \langle r_i \rangle)^2 \rangle}$$

As can be observed, the structural behavior is almost the same for all structures, except for two regions, around the residues number 60 for canine system and 110 for feline system where the fluctuations are expressive. Considering the key residues of *h*ACE2, K31, E35, D38,

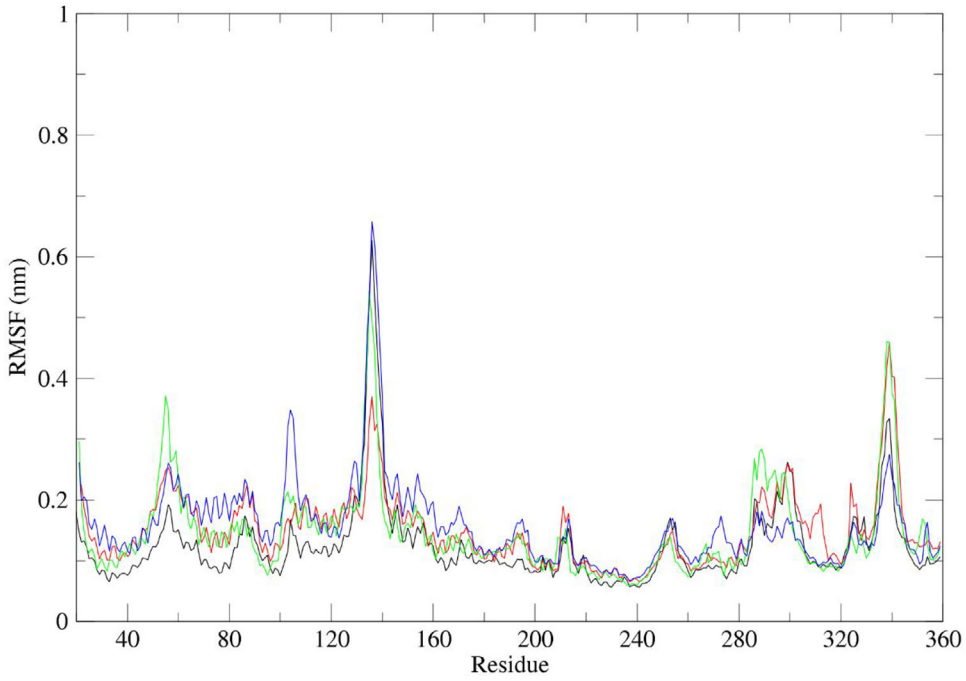

FIGURE 2 Average RMSF for human (black), cat (blue), dog (green), and ferret (red). The complete graphs for the replicas are in the Supporting Information (S30-S6)

TABLE 2 Average RMSF for ACE2 key residues (in bold are those that are shared by all species)

	Key residues				
	Average RMSF (nm)				
Species	K31	E35	D38	M82	K353
Human	0.0833	0.0774	0.0787	0.1216	0.0924
Ferret	0.1171	0.1246	0.1091	0.1832	0.1257
Cat	0.1584	0.1361	0.1253	0.2078	0.1492
Dog	0.1036	0.1006	0.1119	0.1623	0.1685

M82, and K353 (Li et al., 2005; Wan et al., 2020), the average fluctuation for human system residues is 10 times lower than that of the other systems (Table 2).

This behavior, and the average fluctuation of the residues for the human system, suggest that human interface of interaction is more stable, which can also be confirmed by the formation and maintenance of hydrogen bonds along all simulation time (Figure 3).

For cat and dog interaction interfaces, the average number of hydrogen bonds decrease as the simulation is performed, suggesting an adjustment of the residue's positions. For the feline system (Figure S7 in the Supporting Information), considering the three simulations, the behavior is almost the same, only varying the number of hydrogen bonding along the simulation time. For the canine system, there are some differences between the simulations, mainly in the range of 7–15 ns, but the average behavior is the decreasing of the hydrogen bonding number (Figure S8 in the Supporting Information). For the ferret system (Figure S9 in the Supporting Information), the differences between the simulations are more intense than that observed for feline and canine systems, because in one replica, there are two moments, near 20 and 30 ns, that there are no identifiable hydrogen bonds. These results suggest that, for the ferret system, the adjustment of the interaction interface is greater than for the other systems. For the human system (Figure S10 in the Supporting Information), the number of hydrogen bonds along all simulations is basically constant.

Human ACE2 presents five key residues (K31, E35, D38, M82, and K353) while cats, dogs, and ferrets present three (K31, E35, and K353), and an important task is to know what interactions these residues can make, indicating possible sites of inhibition. In order to identify the interactions of these residues, we used the structures obtained from the clustering of each replica. The interaction of all residues for the systems are presented in Table S1 in the Supporting Information, and the principal interactions are in Figures S11–S14 in the Supporting Information.

3.2 | Interacting pair of residues analysis

3.2.1 | Human system

Considering the human system, in all replicas, the key residues of *h*ACE2 had interactions with RBD residues, in agreement with the results of Wan et al. (2020) and Lan et al. (2020). Furthermore, two key residues, E35 and M82, each interacted with only one RBD residue, Q493 and F486, respectively. All other residues had more than one interaction, but the RBD residues were basically the same in all replicas; the only difference was for K31, that had one interaction in Replica

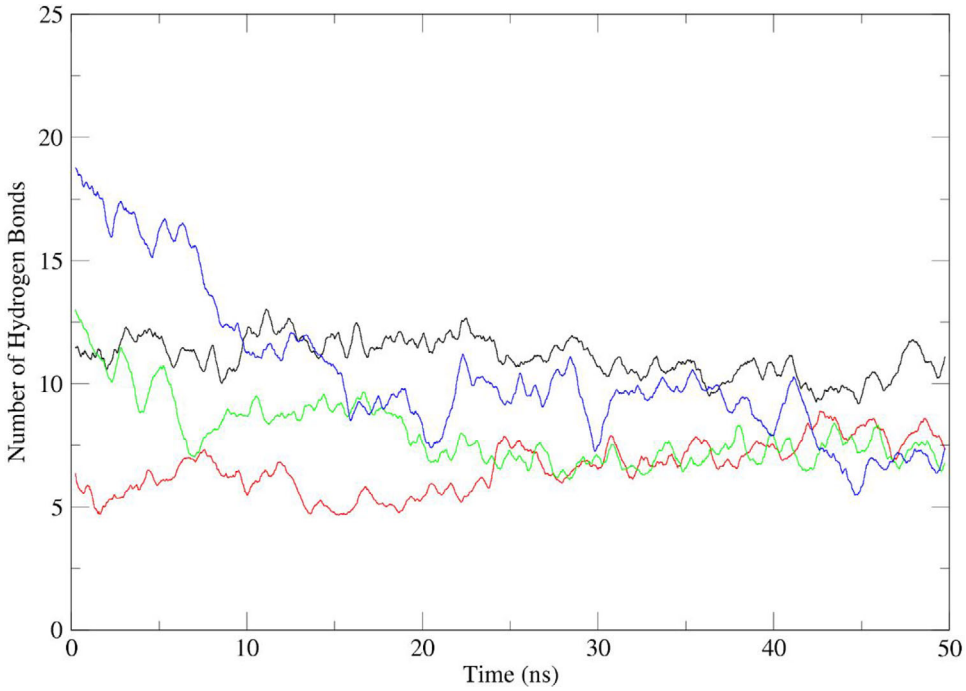

FIGURE 3 Average number of hydrogen bond over time for the simulated systems. Human, cat, dog, and ferret are shown in black, blue, green, and red, respectively

1, and three or four in the others. A long discussion the interaction of human ACE2, SARS-CoV, and SARS-CoV-2, can be found in the work of Ali and Vijayan (2020).

3.2.2 | Dog system

Considering this system, the interactions presented the same pattern that was noted in the other systems: residues from RBD and *d*ACE2 formed more than one interaction. Two of the three key residues, one a hot spot, K31, were found having interactions in all replicas. The interaction pattern shows some residues from RBD that form more than one interaction, such as R466, K462, and L517, for example. From *d*ACE2, E328 and K67 were found to have more than one interaction as well.

3.2.3 | Cat system

In the cat system, among all interacting residues in the RBD, the residues E57, N330, and F72 had several interactions. However, as can be observed in Table S1 in the Supporting Information, the number of interaction residues change between replicas, suggesting that the interaction interface is moving and changing the interacting residues. Considering the key residues in *c*ACE2, there are three of them, K31, E35, and K353. However, K31 only interacts in replica number 3, which is different from the dog system, where $K31_{(dACE2)}$ interacts in all three simulations. The residue K458 from RBD interacts with $E35_{(cACE2)}$ and $K353_{(cACE2)}$, showing differences in interaction pattern between this system and the dog's system.

3.2.4 | Ferret system

In the ferret system, two *f*ACE2 key residues were found: K31 (a hot spot) and E35. The residue F486 from a ferret's RBD seems to be a key residue, because it forms several interactions with different residues in all replicas. The interactions of the two key residues, $K31_{(fACE2)}$:$V445_{(RBD)}$ and $K31_{(fACE2)}$:$G498_{(RBD)}$, as well as $E35_{(fACE2)}$:$G446_{(RBD)}$, $E35_{(fACE2)}$:$G447_{(RBD)}$, and $E35_{(fACE2)}$:$N448_{(RBD)}$, show that the pattern of interaction in all three systems is different.

Along with the analysis of the interacting residues, we extracted from simulations, 10 most persistent hydrogen bonding and among them we showed for how long the key residues, if they appear, maintained their interactions (Figure 4).

3.3 | Hydrogen bond occupancy analysis

3.3.1 | Human system

For the human system, almost all *h*ACE2 key residues are present, showing an occupancy of above 33%. Residues $D38_{(hACE2)}$ and $K353_{(hACE2)}$ interacted with the same RBD residue Q498, but only $D38_{(hACE2)}$ interacted with $Y499_{(RBD)}$. The key residues $E35_{(hACE2)}$, $D38_{(hACE2)}$, and $K353_{(hACE2)}$ presented the most stable interactions,

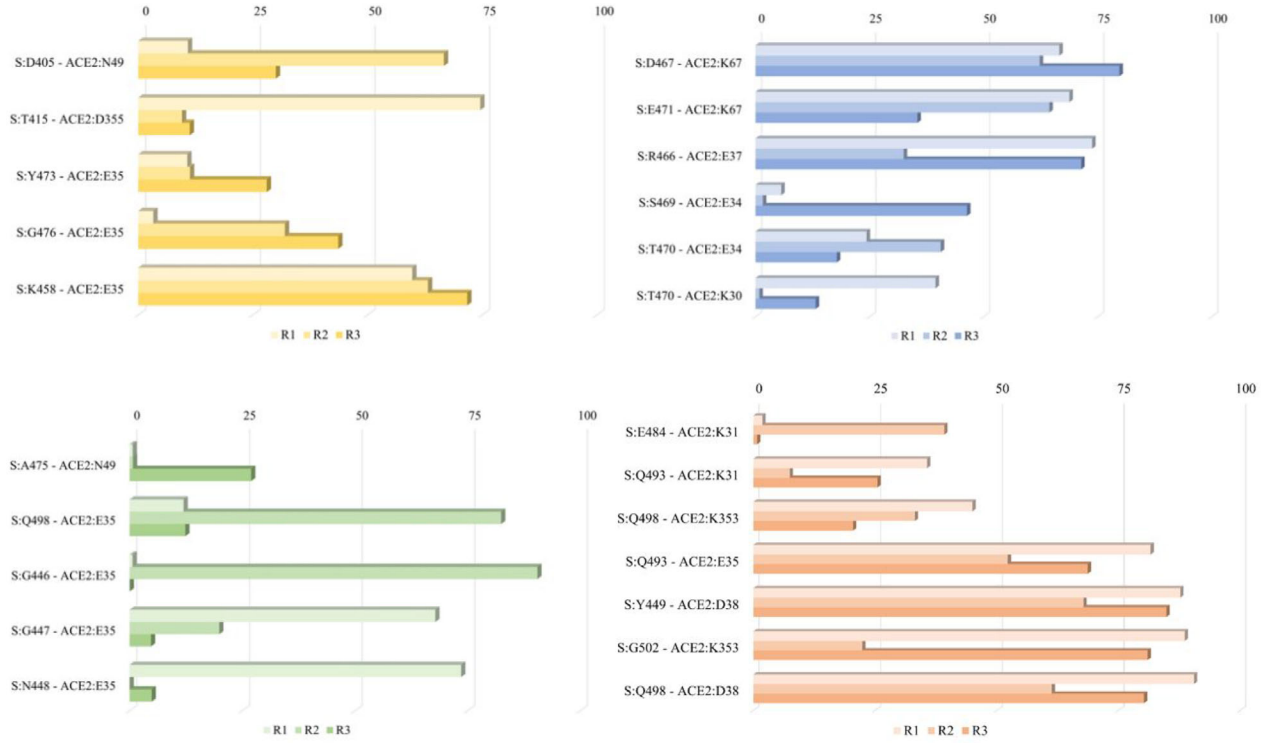

FIGURE 4 Hydrogen bonds occupancy during the simulation time through the replicas. (Yellow for cat system, blue for dog system, green for ferret system, and orange for human system)

forming a group that can contribute to stable interface interaction. The only residue that was not found doing any interaction was $T82_{(hACE2)}$.

3.3.2 | Dog system

For the dog system, $E35_{(dACE2)}$ was the most common interacting residue, as observed in the cat system. However, the occupancy was far below than what was observed in the cat interface, maintaining in all simulations below 50%. This residue interacts in a groove formed by $S470_{(RBD)}$ and $T471_{(RBD)}$ residues. $T471_{(RBD)}$ interacted with another *d*ACE2 key residue, $E30_{(dACE2)}$, that showed an occupancy of almost 40% in the first replica, but did not appear in the other two.

3.3.3 | Cat system

Considering the cat system, hydrogen bond occupancy shows that only the $E35_{(cACE2)}$ key residue is found in them, and presents a maximum occupancy of 71.73% as an acceptor of hydrogen bonding in one replica, and the donor was $K458_{(RBD)}$, that was the most common interacting residue to $E35_{(cACE2)}$, along with $G476_{(RBD)}$, although the occupancy of the latter residue was lower than 50% of the simulation time. Another interaction for the cat system involving $E35_{(cACE2)}$ residue was with $Y473_{(RBD)}$. The $K353_{(cACE2)}$ residue had interactions with $N460_{(RBD)}$ and $K458_{(RBD)}$. $K31_{(cACE2)}$ residue did not have any interactions.

3.3.4 | Ferret system

For the ferret system, the only *f*ACE2 key residue to figure among the first 10 with higher occupancy, was $E35_{(fACE2)}$, showing a maximum value of 90.51% when interacting with $G446_{(RBD)}$. It also interacted with $N448_{(RBD)}$ and $G447_{(RBD)}$ during 79.20% and 67.86% of the simulated time, respectively. Another characteristic of the ferret system was the remarkable difference between replicas, suggesting that this interface is not well established.

4 | DISCUSSION

In this work, homology modeling, molecular docking, and molecular dynamics simulations, involving SARS-CoV-2 RBD and ACE2 from human (*h*ACE2), cat (*c*ACE2), dog (*d*ACE2), and ferret (*f*ACE2) systems, were used in order to evaluate and compare the interaction interface in each system. The interactions and hydrogen bonds in the human system were similar to that found in a recent report (Ali & Vijayan, 2020), suggesting that the interaction interface does not fluctuate as much as those of the pets studied here.

Analyses using ACE2 amino acids homology between animal species and humans have been published (Luan et al., 2020; Zhai et al., 2020) as a tool to predict which animal can be infected by SARS-CoV-2. However, these analyses only show resemblance between the residue sequences, but nothing can be inferred about the dynamic behavior of the systems regarding how they interact and should not be con-

sidered to assess cellular permissiveness to infection, since from the atomistic simulation, the interaction between the RBD and the ACE2 is much more complex than a simple amino acids homology analysis, as has been shown. Furthermore, in these systems, key residues are considered crucial regions of interaction in the process of SARS-CoV and SARS-CoV-2 host cell infection (Li et al., 2005; Wan et al., 2020), and divergences among the key residues in the human (K31, E35, D38, M82, and K353) and animal (K31, E35, and K353) systems were found, which leads to a clue that the interaction between the virus and the cell receptor in dog, cat, and ferret could behave differently.

The COVID-19 pandemic caused by SARS-CoV-2 infections has created an urgent need for treatment and vaccine research, which require testing in appropriate animal models of the disease. An ideal animal model of a human disease is one in which the pattern of infection is similar to that which occurs in humans (Cleary et al., 2020). Our results show that human interface of interaction is more stable, and there are differences in their interaction modes and binding pattern compared to pet's systems that suggest that the use of dog, cat, or ferret as experimental models will not reflect what happens during infection in humans, so results obtained using in vivo experiments with these species may not be applicable to addressing COVID-19. Additionally, the pathogenicity and high susceptibility to SARS-CoV and SARS-CoV-2 were reproduced only in transgenic mice that express human ACE2 (*h*ACE2), and not in wild-type mice (*m*ACE2), concluding that *h*ACE2 was essential for SARS-CoV-2 infection and replication in mice (Bao et al., 2020; McCray et al., 2007; Netland et al., 2008; Sun et al., 2020), which by analogy can be extended to the data found here for dog, cat, and ferret. Studies using SARS-CoV experimental infection in transgenic dog, cat, or ferret model expressing *h*ACE2 were not found.

Dogs and cats do not suffer from the presence of SARS-CoV-2, showing an absence of persistent infection and clinical signs (Hosie et al, 2020; Sit et al., 2020), which can be suggested, from an atomistic point of view, by the differences in interactions observed in our results. Furthermore, SARS-CoV-2 led to acute bronchiolitis in experimentally infected ferrets; however, fatalities were not observed (Kim et al., 2020), and reports of natural infections in this species were not found; high-affinity virus receptor interaction might be one of the crucial factors that determines the virulence of this pathogen in the host (Sarkar & Guha, 2020). Ferrets are experimental models of respiratory viruses often used in laboratories, and are also kept as pets with some popularity in certain countries. Under natural conditions, 29 ferrets in prolonged and direct contact with two humans with COVID-19 proved that they are resistant to infection, with no detection of viral RNA (RT-qPCR), and no RBD-specific seroconversion (ELISA) (Sawatzki et al., 2021).

Beyond the question of these species as animal models, the possibility of detection of SARS-CoV-2 in companion animals has generated concerns about abandonment (Hora, 2020; Huang et al., 2020). Cat and dog populations are extremely large in several countries, and the increase of these animals circulating in the streets could result in serious consequences to public health, in addition to questions related to animal welfare. Results obtained in this work suggest a very low-level participation of these animals in pandemic maintenance, which is supported by reports stating that natural infections are rarely observed in dogs and cats (fewer than 200 cases), and absent in ferrets. Considering the world population of dogs and cats kept as pets, the number of infected animals already reported is irrelevant in the pandemic context.

5 | CONCLUSIONS

In this work, molecular dynamics simulations were used to study the interaction interface between SARS-CoV-2-RBD and ACE2 from humans, cats, dogs, and ferrets in order to identify commonalities across species. The analysis of the structural results suggest that the interaction interface of the human system is more stable, corroborated by differences in the fluctuation values of the key residues and the behavior of the hydrogen bonds along the simulation time. The differences in the number of interactions made by key residues during the replicas, between the systems, suggest that the infection process in humans is more effective. Additionally, the hydrogen bonds formed over time present high differences in the occupancy time during the simulation, showing that the human RBD-*h*ACE2 interface can be considered more stable among the studied systems. Furthermore, the few reports of natural occurrence of SARS-CoV-2 in pet animals worldwide suggest that infection in them occurs rarely, and the results discussed here can help evaluate the reasons for these numbers. In addition, our data suggest that the use of dogs, cats, and ferrets as experimental models for treatment and vaccines for SARS-CoV-2 should be considered cautiously, if not actively discouraged.

ACKNOWLEDGEMENT

The authors want to thank Cesar Simenes who allowed the simulations to be done in the Orion Computer at UFU-Ituiutaba.

CONFLICT OF INTEREST

The authors confirm that there is no conflict of interest.

ETHICS STATEMENT

The authors declare that ethics statements are not applicable for this work. There were no questionnaires or sample collections. All used information was retrieved from published articles.

DATA AVAILABILITY STATEMENT

Data sharing not applicable—the article describes entirely theoretical research.

REFERENCES

Abraham, M. J., Murtola, T., Schulz, R., Páll, S., Smith, J. C., Hess, B., & Lindah, E. (2015). Gromacs: High performance molecular simulations through multi-level parallelism from laptops to supercomputers. *SoftwareX*, *1-2*, 19–25. https://doi.org/10.1016/j.softx.2015.06.001

Ali, A., & Vijayan, R. (2020). Dynamics of the ACE2–SARS-CoV-2/SARS-CoV spike protein interface reveal unique mechanisms. *Scientific Reports*, *10*, 14214. https://doi.org/10.1038/s41598-020-71188-3

Arantes, P. R., Saha, A., & Palermo, G. (2020). Fighting COVID-19 using molecular dynamics simulations. *ACS Central Science*, *6*, 1654–1656. https://doi.org/10.1021/acscentsci.0c01236

Bao, L., Deng, W., Huang, B., Gao, H., Liu, J., Ren, L., Wei, Q., Yu, P., Xu, Y., Qi, F., Qu, Y., Li, F., Lv, Q., Wang, W., Xue, J., Gong, S., Liu, M., Wang, G., Wang, S., … Qin, C. (2020). The pathogenicity of SARS-CoV-2 in hACE2 transgenic mice. *Nature*, *583*, 830–833. https://doi.org/10.1038/s41586-020-2312-y

Basu, A., Sarkar, A., & Maulik, U. (2020). Molecular docking study of potential phytochemicals and their effects on the complex of SARS-CoV2 spike protein and human ACE2. *Scientific Reports*, *10*, 17699. https://doi.org/10.1038/s41598-020-74715-4

Berendsen, H. J. C., Postma, J. P. M., Van Gunsteren, W. F., Dinola, A., & Haak, J. R. (1984). Molecular dynamics with coupling to an external bath. *Journal of Chemical Physics*, *81*, 3684–3690. https://doi.org/10.1063/1.448118

Bussi, G., Donadio, D., & Parrinello, M. (2007). Canonical sampling through velocity rescaling. *Journal of Chemical Physics*, *126*, 014101. https://doi.org/10.1063/1.2408420

Cleary, S. J., Pitchford, S. C., Amison, R. T., Carrington, R., Cabrera, C. L. R., Magnen, M., Looney, M. R., Gray, E., & Page, C. P. (2020). Animal models of mechanisms of SARS-CoV-2 infection and COVID-19 pathology. *British Journal of Pharmacology*, *177*, 4851–4865. https://doi.org/10.1111/bph.15143

Cui, J., Li, F., & Shi, Z. L. (2019). Origin and evolution of pathogenic coronaviruses. *Nature Reviews Microbiology*, *17*, 181–192. https://doi.org/10.1038/s41579-018-0118-9

Gapper, J. (2019, July 31). Pets are making Wall Street wag its tail. *Financial Times*. https://www.ft.com/content/703ae54c-b2ad-11e9-8cb2-799a3a8cf37b

Hall, T. A. (1999). BioEdit: A user-friendly biological sequence alignment editor and analysis program for Windows 95/98/NT. *Nucleic Acids Symposium Series*, *41*, 95–98. https://doi.org/10.14601/PHYTOPATHOL_MEDITERR-14998U1.29

Hess, B., Bekker, H., Berendsen, H. J. C., & Fraaije, J. G. E. M. (1997). LINCS: A linear constraint solver for molecular simulations. *Journal of Computational Chemistry*, *18*, 1463–1472. https://doi.org/10.1002/(SICI)1096-987X(199709)18:12<1463::AID-JCC4>3.0.CO;2-H

Hoover, W. G. (1985). Canonical dynamics: Equilibrium phase-space distributions. *Physical Review A*, *31*, 1695–1697. https://doi.org/10.1103/PhysRevA.31.1695

Hora, A. S. (2020). Coronavirus: A veterinary perspective. *Nature*, *580*, 321. https://doi.org/10.1038/d41586-020-01077-2

Hosie, M. J., Hartmann, K., Hofmann-Lehmann, R., Addie, D. D., Truyen, U., Egberink, H., Tasker, S., Frymus, T., Pennisi, M. G. & K. M. (2020). SARS-Coronavirus (CoV)-2 and cats. European Advisory Board on Cat Diseases. http://www.abcdcatsvets.org/sars-coronavirus-2-and-cats/

Huang, Q., Zhan, X., & Zeng, X. T. (2020). COVID-19 pandemic: Stop panic abandonment of household pets. *Journal of Travel Medicine*, *27*, taaa046. https://doi.org/10.1093/jtm/taaa046

Humphrey, W., Dalke, A., & Schulten, K. (1996). VMD: Visual molecular dynamics. *Journal of Molecular Graphics*, *14*, 33–38. https://doi.org/10.1016/0263-7855(96)00018-5

Jorgensen, W. L., Chandrasekhar, J., Madura, J. D., Impey, R. W., & Klein, M. L. (1983). Comparison of simple potential functions for simulating liquid water. *Journal of Chemical Physics*, *79*, 926–935. https://doi.org/10.1063/1.445869

Jorgensen, W. L., & Tirado-Rives, J. (1988). The OPLS potential functions for proteins. Energy minimizations for crystals of cyclic peptides and crambin. *Journal of the American Chemical Society*, *110*, 1657–1666. https://doi.org/10.1021/ja00214a001

Kim, Y. I., Kim, S. G., Kim, S. M., Kim, E. H., Park, S. J., Yu, K. M., Chang, J. H., Kim, E. J., Lee, S., Casel, M. A. B., Um, J., Song, M. S., Jeong, H. W., Lai, V. D., Kim, Y., Chin, B. S., Park, J. S., Chung, K. H., Foo, S. S., … Choi, Y. K. (2020). Infection and rapid transmission of SARS-CoV-2 in ferrets. *Cell Host & Microbe*, *27*, 704–709. https://doi.org/10.1016/j.chom.2020.03.023

Lan, J., Ge, J., Yu, J., Shan, S., Zhou, H., Fan, S., Zhang, Q., Shi, X., Wang, Q., Zhang, L., & Wang, X. (2020). Structure of the SARS-CoV-2 spike receptor-binding domain bound to the ACE2 receptor. *Nature*, *581*, 215–220. https://doi.org/10.1038/s41586-020-2180-5

Laskowski, R. A., MacArthur, M. W., Moss, D. S., & Thornton, J. M. (1993). PROCHECK: A program to check the stereochemical quality of protein structures. *Journal of Applied Crystallography*, *26*, 283–291. https://doi.org/10.1107/s0021889892009944

Li, F. (2015). Receptor recognition mechanisms of coronaviruses: A decade of structural studies. *Journal of Virology*, *89*, 1954–1964. https://doi.org/10.1128/jvi.02615-14

Li, F., Li, W., Farzan, M., & Harrison, S. C. (2005). Structural biology: Structure of SARS coronavirus spike receptor-binding domain complexed with receptor. *Science*, *309*, 1864–1868. https://doi.org/10.1126/science.1116480

Li, W., Moore, M. J., Vasllieva, N., Sui, J., Wong, S. K., Berne, M. A., Somasundaran, M., Sullivan, J. L., Luzuriaga, K., Greeneugh, T. C., Choe, H., & Farzan, M. (2003). Angiotensin-converting enzyme 2 is a functional receptor for the SARS coronavirus. *Nature*, *426*, 450–454. https://doi.org/10.1038/nature02145

Li, W., Wong, S-K., Li, F., Kuhn, J. H., Huang, I-C., Choe, H., & Farzan, M. (2006). Animal origins of the severe acute respiratory syndrome coronavirus: Insight from ACE2-S-protein interactions. *Journal of Virology*, *80*, 4211–4219. https://doi.org/10.1128/jvi.80.9.4211-4219.2006

Luan, J., Lu, Y., Jin, X., & Zhang, L. (2020). Spike protein recognition of mammalian ACE2 predicts the host range and an optimized ACE2 for SARS-CoV-2 infection. *Biochemical and Biophysical Research Communications*, *526*, 165–169. https://doi.org/10.1016/j.bbrc.2020.03.047

Mallapaty, S. S. (2020). Coronavirus can infect cats — dogs, not so much. *Nature*. https://doi.org/10.1038/d41586-020-00984-8

McCray, P. B., Pewe, L., Wohlford-Lenane, C., Hickey, M., Manzel, L., Shi, L., Netland, J., Jia, H. P., Halabi, C., Sigmund, C. D., Meyerholz, D. K., Kirby, P., Look, D. C., & Perlman, S. (2007). Lethal infection of K18- hACE2 mice infected with severe acute respiratory syndrome coronavirus. *Journal of Virology*, *81*, 813–821. https://doi.org/10.1128/JVI.02012-06

Morens, D. M., Daszak, P., & Taubenberger, J. K. (2020). Escaping Pandora's box — Another novel coronavirus. *New England Journal of Medicine*, *382*, 1293–1295. https://doi.org/10.1056/NEJMp2002106

Netland, J., Meyerholz, D. K., Moore, S., Cassell, M., & Perlman, S. (2008). Severe acute respiratory syndrome coronavirus infection causes neuronal death in the absence of encephalitis in mice transgenic for human ACE2. *Journal of Virology*, *82*, 7264–7275. https://doi.org/10.1128/JVI.00737-08

Nosé, S., & Klein, M. L. (1983). Constant pressure molecular dynamics for molecular systems. *Molecular Physics*, *50*, 1055–1076. https://doi.org/10.1080/00268978300102851

Nosé, S. (1984). A unified formulation of the constant temperature molecular dynamics methods. *Journal of Chemical Physics*, *81*, 511–519. https://doi.org/10.1063/1.447334

Parrinello, M., & Rahman, A. (1981). Polymorphic transitions in single crystals: A new molecular dynamics method. *Journal of Applied Physics*, *52*, 7182–7190. https://doi.org/10.1063/1.328693

Perilla, J. R., & Schulten, K. (2017). Physical properties of the HIV-1 capsid from all-atom molecular dynamics simulations. *Nature Communications*, *8*, 15959. https://doi.org/10.1038/ncomms15959

Razzaghi-Asl, N., Ebadi, A., Shahabipour, S., & Gholamin, D. (2020). Identification of a potential SARS-CoV2 inhibitor via molecular dynamics simulations and amino acid decomposition analysis. *Journal of Biomolecular Structure & Dynamics*, 1–16. https://doi.org/10.1080/07391102.2020.1797536

Sarkar, J., & Guha, R. (2020). Infectivity, virulence, pathogenicity, host-pathogen interactions of SARS and SARS-CoV-2 in experimental animals: A systematic review. *Veterinary Research Communications*, *44*, 101–110. https://doi.org/10.1007/s11259-020-09778-9

Sawatzki, K., Hill, N. J., Puryear, W. B., Foss, A. D., Stone, J. J., & Runstadler, J. A. (2021). Host barriers to SARS-CoV-2 demonstrated by ferrets in a high-exposure domestic setting. *PNAS*, *118*, e2025601118. https://doi.org/10.1073/pnas.2025601118

Shi, J., Wen, Z., Zhong, G., Yang, H., Wang, C., Huang, B., Liu, R., He, X., Shuai, L., Sun, Z., Zhao, Y., Liu, P., Liang, L., Cui, P., Wang, J., Zhang, X., Guan, Y., Tan, W., Wu, G., … Bu, Z. (2020). Susceptibility of ferrets, cats, dogs, and other domesticated animals to SARS-coronavirus 2. *Science*, *368*, 1016–1020. https://doi.org/10.1126/science.abb7015

Sit, T. H. C., Brackman, C. J., Ip, S. M., Tam, K. W. S., Law, P. Y. T., To, E. M. W., Yu, V. Y. T., Sims, L. D., Tsang, D. N. C., Chu, D. K. W., Perera, R. A. P. M., Poon, L. L. M., & Peiris, M. (2020). Infection of dogs with SARS-CoV-2. *Nature*, *586*, 776–778. https://doi.org/10.1038/s41586-020-2334-5

Sun, S-H., Chen, Q., Gu, H-J., Yang, G., Wang, Y-X., Huang, X-Y., Liu, S-S., Zhang, N-N., Li, X.-F., Xiong, R., Guo, Y., Deng, Y.-Q., Huang, W.-J., Liu, Q., Liu, Q.-M., Shen, Y.-L., Zhou, Y., Yang, X., Zhao, T.-Y., … & Wang, Y.-C. (2020). A mouse model of SARS-CoV-2 infection and pathogenesis. *Cell Host & Microbe*, *28*, 124–133.e4. https://doi.org/10.1016/j.chom.2020.05.020

Van Zundert, G. C. P., Rodrigues, J. P. G. L. M., Trellet, M., Schmitz, C., Kastritis, P. L., Karaca, E., Melquiond, A. S. J., Van Dijk, M., De Vries, S. J., & Bonvin, A. M. J. J. (2016). The HADDOCK2.2 web server: User-friendly integrative modeling of biomolecular complexes. *Journal of Molecular Biology*, *428*, 720–725. https://doi.org/10.1016/j.jmb.2015.09.014

Wan, Y., Shang, J., Graham, R., Baric, R. S., & Li, F. (2020). Receptor recognition by the novel coronavirus from Wuhan: An analysis based on decade-long structural studies of SARS coronavirus. *Journal of Virology*, *94*, e00127–20. https://doi.org/10.1128/JVI.00127-20

Waterhouse, A., Bertoni, M., Bienert, S., Studer, G., Tauriello, G., Gumienny, R., Heer, F. T., De Beer, T. A. P., Rempfer, C., Bordoli, L., Lepore, R., & Schwede, T. (2018). SWISS-MODEL: Homology modelling of protein structures and complexes. *Nucleic Acids Research*, *46*, W296–W303. https://doi.org/10.1093/nar/gky427

Wu, F., Zhao, S., Yu, B., Chen, Y.-M., Wang, W., Song, Z.-G., Hu, Y., Tao, Z.-W., Tian, J.-H., Pei, Y.-Y., Yuan, M.-L., Zhang, Y.-L., Dai, F.-H., Liu, Y., Wang, Q.-M., Zheng, J.-J., Xu, L., Holmes, E. C., & Zhang, Y.-Z. (2020). A new coronavirus associated with human respiratory disease in China. *Nature*, *579*, 265–269. https://doi.org/10.1038/s41586-020-2008-3

Zhai, X., Sun, J., Yan, Z., Zhang, J., Zhao, J., Zhao, Z., Gao, Q., He, W.-T., Veit, M., & Su, S. (2020). Comparison of severe acute respiratory syndrome coronavirus 2 spike protein binding to ACE2 receptors from human, pets, farm animals, and putative intermediate hosts. *Journal of Virology*, *94*, e00831–20. https://doi.org/10.1128/JVI.00831-20

Zhou, P., Yang, X. L. X.-L., Wang, X. G. X.-G., Hu, B., Zhang, L., Zhang, W., Si, H. R. H.-R., Zhu, Y., Li, B., Huang, C.-L. C. L., Chen, H. D. H.-D., Chen, J., Luo, Y., Guo, H., Jiang, R. D. R.-D., Liu, M. Q. M.-Q., Chen, Y., Shen, X. R. X.-R., Wang, X. G. X.-G., … & Shi, Z. L. Z.-L. (2020). A pneumonia outbreak associated with a new coronavirus of probable bat origin. *Nature*, *579*, 270–273. https://doi.org/10.1038/s41586-020-2012-7

Zhu, N., Zhang, D., Wang, W., Li, X., Yang, B., Song, J., Zhao, X., Huang, B., Shi, W., Lu, R., Niu, P., Zhan, F., Ma, X., Wang, D., Xu, W., Wu, G., Gao, G. F., Tan, W., & China Novel Coronavirus Investigating and Research Team. (2020). A novel coronavirus from patients with pneumonia in China. (2019). *New England Journal of Medicine*, *382*, 727–733. https://doi.org/10.1056/NEJMoa2001017

SUPPORTING INFORMATION

Additional supporting information may be found online in the Supporting Information section at the end of the article.

How to cite this article: Soté, W. O., Franca, E. F., Hora, A. S., & Comar, M. (2022). A computational study of the interface interaction between SARS-CoV-2 RBD and ACE2 from human, cat, dog, and ferret. *Transboundary and Emerging Diseases*, *69*, 2287–2295. https://doi.org/10.1111/tbed.14234